Hole and Electron Transport in Chloroaluminum Phthalocyanine Thin Films

A. Ioannidis and J. P. Dodelet*

INRS-Énergie et Matériaux, 1650 Lionel Boulet, C.P. 1020 Varennes, Québec, Canada J3X 1S2

Received: January 7, 1997; In Final Form: April 6, 1997[⊗]

Thin films (∼1.2 μm) of chloroaluminum phthalocyanine (ClAlPc) are vacuum sublimed at sublimation rates of 200 and 1000 Å/min on substrates maintained at two temperatures, T_s = 25 and 95 °C. Hole mobilities are very well described by the disorder formalism of Bässler and co-workers. As sublimation rate decreases or T_s increases, σ, the width of density of states, decreases to a minimum of 0.052 eV. "Intrinsic" mobility, μ_{00}, increases concomitantly, as do measured mobilities, reaching $\sim 1 \times 10^{-3}$ cm^2/(V s). Positional disorder, Σ, is less affected by the sublimation conditions. Results, as discussed in the context of previous work, indicate an increased organization of molecules in slowly deposited films on heated substrates. An anomalous increase of mobilities, as temperature decreases below a reversal temperature, is confirmed for all samples. The reversal temperature itself increases with increased film organization, from 213 to 253 K, consistent with greater coplanar overlap of Pc macrocycles on cooling. Electron transport is observed in these amorphous/polycrystalline phthalocyanine thin films, without specific film treatments. Mobilities under primary vacuum and their dependencies are comparable for electrons and holes. Similar σ and μ_{00} as for holes but larger Σ are obtained in a given sample. A negative temperature dependence of the mobilities is also observed for electrons at low temperatures. Measurements of electron mobilities in ClAlPc films are impeded by the presence of air and favored by a better molecular organization in the films.

Introduction

Metal phthalocyanines (MPcs) have a main high technology commercial application as photogenerating materials in electrophotography due to their intense absorption in the visible (extending to the near infrared), their chemical stability under illumination, and their relatively low cost.[1−3] Photogeneration properties have therefore been well documented,[4−8] demonstrating that the first excited singlet state is the precursor of geminate electron−hole pairs, which can then lead to free carriers. The situation is more obscure concerning any subsequent transport of the charge carriers through the bulk materials, as various phases spanning single crystal to amorphous are obtainable, with various degrees of purity. This large variety in transport environments then accounts for the fact that descriptions of charge transport properties in MPcs span the range from delocalized carrier transport (band model)[9−12] to thermally activated hopping.[12−16,17]

In the case of phthalocyanine thin films, which tend to be largely amorphous, mobilities have traditionally been deduced from space-charge-limited current techniques, deep trapping of carriers by molecular oxygen, or impurities, making direct time-of-flight (TOF) measurements problematic.[3a,18] At best, TOF has produced very dispersive transients, which give mobilities that are difficult to interpret.[14,19] Recently however, attention to purification and sample preparation procedures allowed us to observe TOF transients with only moderate dispersivity throughout a full range of fields and temperatures in vacuum-sublimed (deposition rate of ∼2000 Å/min) rather amorphous thin films of chloroaluminum phthalocyanine (ClAlPc).[20,21] Similar results were obtained in thin films of chlorogallium and chloroindium phthalocyanines (ClGaPc and ClInPc).[21] Interest has been focused on this trivalent group of MPcs due to their particularly high photoactivity and charge generation efficiency (refs 2, 3, 22, and references therein), particularly in ClAlPc, which is able, with chemical and structural modifications, to generate photocurents in the mA/cm^2 range.[22,23]

The previous results of mobility measurements in ClAlPc were successfully modeled according to the disorder formalism due to Bässler and co-workers.[24−26] This formalism has been widely used to describe charge transport in organic amorphous materials of interest to xerography.[18] Charge transport is considered to occur by hopping within a manifold of localized states subject to Gaussian distributions of site energies and of relative distances and molecular orientations ("positions"). The two central parameters are σ and Σ; σ, the energy width of the density of states is related to the energetic disorder $\hat{\sigma} = \sigma/kT$, while Σ is a measure of positional disorder. Energetic and positional disorder contribute independently to the mobility, μ. The formalism predicts (a) a Poole−Frenkel type[27] field dependence of the mobility as $\ln \mu \propto SE^{1/2}$ at fields above 10^5 V/cm;[28,29] (b) a temperature dependence of the form $\ln \mu \propto 1/T^2$; (c) a temperature dependence of the field dependencies whereby the high-field slopes, S, of the $\ln \mu \propto E^{1/2}$ relation increase with decreasing temperatures such that $S \propto \sigma^2$, with a slope $C = 2.9 \times 10^{-4}$ (cm/V)$^{1/2}$; and (d) a nondispersive to dispersive (ND−D) transition at low temperatures.[30] The parameters σ and Σ can be extracted from the dependencies in b and c, respectively.

For ClAlPc, the parameters of energetic and positional disorder calculated in the previous work[20] reflect an increase in film organization that was achieved by increasing substrate temperatures during film depositions. This led to an order of magnitude increase in room temperature mobility, saturating at values in the low 10^{-4} cm^2/(V s). At the same time, mobilities were found to increase with decreasing temperatures from ∼200 to 93 K.[21] This effect was common to the trivalent group of Cl(M)Pcs, where M = Al, Ga, or In.

In the present work, the film deposition rate of ClAlPc is decreased and/or the substrate temperature is increased, to examine their effects on film organization and mobility. A further order of magnitude increase in hole mobility to the 10^{-3} cm^2/(V s) range is obtained. The anomalous low-temperature reversal of mobilities is ubiquitous, and trends in this reversal

[⊗] Abstract published in *Advance ACS Abstracts,* June 1, 1997.

S1089-5647(97)00112-0 CCC: $14.00

and in increasingly inverse field dependencies with sample type will be discussed. The disorder formalism will be seen to continue to provide a meaningful framework for the discussion of charge transport in the more ordered films now studied.

Finally, electron transients are measured in the same thin films of ClAlPc, showing similar profiles to the hole transients and mobility values of magnitude similar to the hole mobilities. Apart from purity and exposure to oxygen, the increased organization of the material and its effect on the transport of charge carriers may play an important role in electron transport. Disorder parameters obtained from electron and hole results will be discussed in terms of different sites for electron and hole transport in ClAlPc. The same trends appear as for the hole mobilities and are more pronounced.

Experimental Section

A. ClAlPc Synthesis and Sample Preparation. ClAlPc was synthesized according to a procedure similar to that described by Owens and Kenny.[31] The product was purified by sublimation twice in a vacuum of 10^{-5} Torr and a temperature of 510 °C. Details of synthesis and purification procedures as well as elemental analysis have been reported elsewhere.[22]

Vacuum sublimed ~1.2 μm thick films of ClAlPc were incorporated in an Al/ClAlPc/Al sandwich cell structure, as described previously.[20] Films were vacuum sublimed under three sets of deposition conditions, varying the temperature T_s at which substrates were maintained during deposition and/or the deposition rate ("rate"):

S1 was obtained with $T_s = 95$ °C, rate ≈ 1000 Å/min

S2 was obtained with $T_s = 25$ °C, rate ≈ 200 Å/min

S3 was obtained with $T_s = 95$ °C, rate ≈ 200 Å/min

A batch of three or four samples was prepared at each set of conditions.

Film deposition at $T_s = 95$ °C and 200 Å/min was slightly modified in order to solve a problem of short-circuiting of the Al contacts through pinholes in the film. The deposition rate was therefore briefly increased at the end of the film depositions to produce a very thin (~0.1 μm) amorphous layer at the top (illuminated) surface of the films in order to block the pinholes. This is simply equivalent to using a separate charge generation layer to inject charges into the bulk of the film. The modified films worked very well at thicknesses of 1.2 μm or above, while for thinner films this combination of layers produced very dispersive transients, which may be expected.

B. Mobility Measurements. Mobilities of samples placed in a vacuum chamber at 10^{-3}−10^{-2} Torr were determined by a conventional time-of-flight technique.[32,33] Experimental conditions have been previously detailed (ref 20 and references therein. Figure 1 shows a typical photocurrent transient. Transient profiles showed different degrees of moderate dispersivity according to sample and to field but always displayed a small plateau or knee. A tail-broadening parameter can be defined according to[34]

$$W = (t_{1/2} - t_t)/t_{1/2} \quad (1)$$

where $t_{1/2}$ is the time for the current to decay to 1/2 its value at the transit time, t_t. This gives $W = 0.5$ in Figure 1. W increased weakly with field and falling temperatures for all samples.

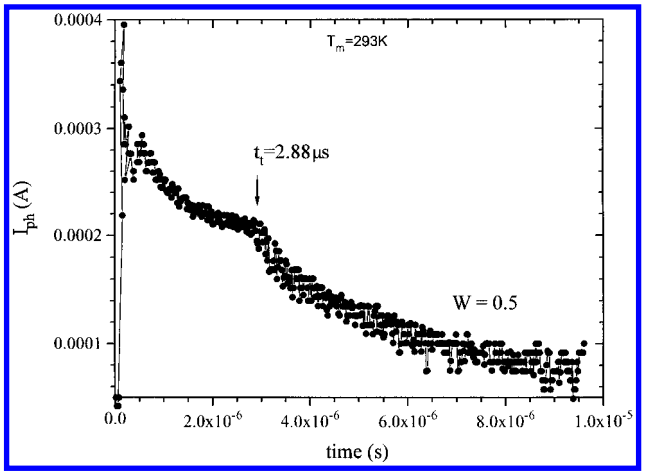

Figure 1. Typical hole transient featuring distinct plateau for transit time (t_t) determination. Sample type was S3, thickness $L = 1.2$ μm, field $E = 3.3 \times 10^4$ V/cm, yielding mobility $\mu = L/Et_t = 1.25 \times 10^{-3}$ cm^2/(V s).

Logarithmic representations of transients were used to determine transit times, for consistency when comparing to previous results.[20,21]

Mobilities were measured with illuminated electrode positive for holes and illuminated electrode negative for electrons. The range of fields was limited at the high end by the resolution of the experimental arrangement and at the low end by signal-to-noise considerations. Measurement temperatures for the present sample series ranged from 333 K to as low as 73 K. Photocurrent transients were obtained in triplicate at each field setting and averaged while repeat field and temperature runs were performed on each sample. Representative results for one sample from each type will be presented.

Results

Measurements and calculations are organized as follows: In the upper range of measurement temperatures, hole mobilities were analyzed in the framework of the disorder formalism. Disorder parameters were calculated[34,35] for each set of deposition conditions (S1−S3) from the deconvoluted temperature and field dependencies. Hole mobilities as a function of field for lower temperatures are then presented in comparison for each sample. Similar treatment is applied to electron mobility measurements, with analytical results presented for the least and most ordered samples in the series (S1 and S3, respectively). As an aid to readability, substrate temperatures T_s will be reported in units of Celsius and measurement temperatures T_m in units of kelvin.

A. Hole Mobilities. Figure 2 shows the field dependence of mobility, μ, obtained at $T_m = 293$ K for films deposited on substrates held at $T_s = 25$ °C and 95 °C. In this figure, mobilities for the films deposited at the present rate = 1000 and 200 Å/min (S1−S3) can be compared to those at previous rate = 2000 Å/min (C1, C2).[20] It is immediately apparent that mobilities increase with either substrate temperature or lowering of deposition rate. The combination in S3 of highest substrate temperature and lowest deposition rate yields the highest mobilities (~1×10^{-3} cm^2/(V s)). Furthermore, starting with C1, a low mobility sample, the greater increase in mobility is obtained by decreasing the rate to 200 Å/min (S2) compared to heating the substrate to $T_s = 95$ °C (C2). Note that, as far as film organization and mobility is concerned, it has been shown previously that heating the substrate to this temperature is equivalent to heating it to any temperature from 80 to 180 °C.[20,22] Differences in the field dependencies of mobility for

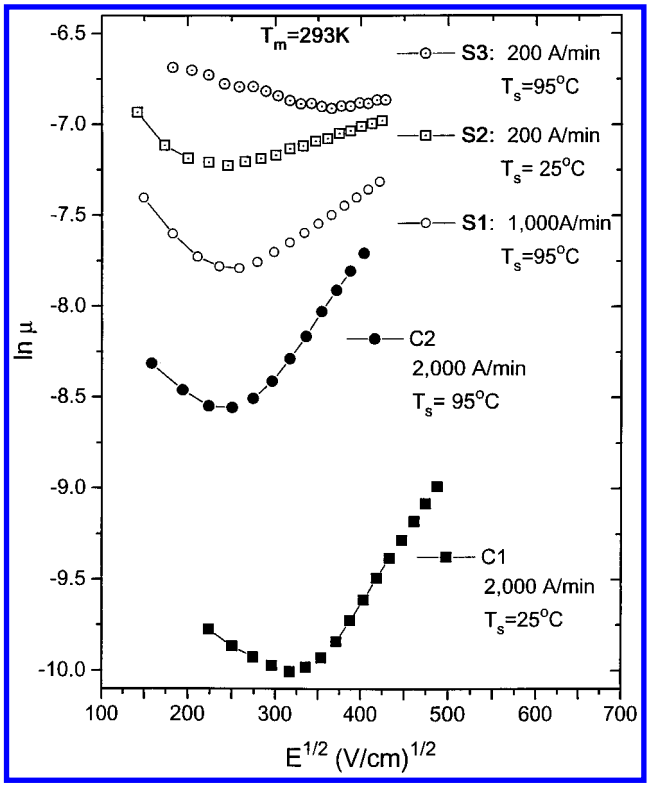

Figure 2. Comparison of hole mobilities at different fields for a given T_m (293 K) in present sample types S1−S3 and two relevant types previously studied, C1 and C2. The overall increase in mobilities from C1 to S3 is ∼2 orders of magnitude.

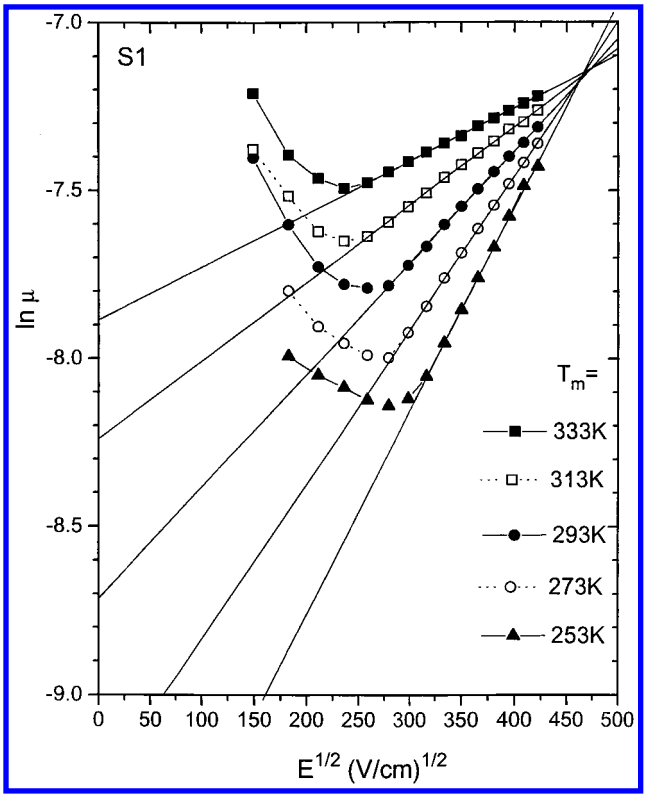

Figure 3. Field dependence of hole mobility at high temperatures T_m = 333−253 K for S1 (T_s = 95 °C, rate = 1000Å/min). The relation ln $\mu \propto SE^{1/2}$ is followed for E above ∼6.5 × 10^4 V/cm. An inverse field dependence applies for E below ∼(5.5−6) × 10^4 V/cm.

S1−S3 were found to translate to different disorder parameters for each sample, calculated below.

Figure 3 shows the field dependence of mobility at T_m = 333−253 K for S1 (T_s = 95 °C and rate = 1000 Å/min). Results in this T_m range were reversible with no signs of hysteresis. Extrapolation of the observed linear high-field behavior (ln $\mu \propto SE^{1/2}$) to zero field gives the zero-field mobility, $\mu_{E=0}$. Using $\mu_{E=0}$, the energetic width of the density of states, σ, is calculated according to the relation

$$\mu_{E=0} = \mu_o \exp -(2\sigma/3kT_m)^2 \qquad (2)$$

A linear plot of ln $\mu_{E=0}$ versus $1/T_m^2$ was obtained, whose slope yielded σ. The zero-temperature intercept gives the prefactor mobility μ_o. The positional disorder parameter Σ can be determined from the temperature dependence of the slopes, S, in Figure 3. Simulations predict that S versus $\hat{\sigma}^2$ should be linear. The energetic disorder $\hat{\sigma}$ is defined as

$$\hat{\sigma} = \sigma/kT_m \qquad (3)$$

Σ is then determined at the $S = 0$ intercept, from the condition $\hat{\sigma}^2 = \Sigma^2$.

A linear plot was obtained whose slope was denoted as "C". The disorder parameters of S1 are summarized in Table 1 with those of all samples.

The field dependencies of mobility from 293 to 93 K for S1 are presented in three parts in Figure 4a,b,c to compare the "high", "transitional", and "low" temperature ranges indicated in the figure. Figure 4a illustrates the usual decrease in mobility with temperature down to 233 K. In Figure 4b, the mobility at 213 K is very close to that at 233 K. Figure 4c demonstrates a clear *negative temperature dependence of mobility* from T_m = 213−93 K for all fields. Results from 233 to 93 K were reversible but with a hysteresis of several hours.

Figure 5 shows the field dependence of mobility at T_m = 333−273 K for S2 (T_s = 25 °C, rate = 200 Å/min). The experimental range amenable to calculation was therefore restricted by 20 K compared to S1. Results were reproducible with no sign of hysteresis. The mobility field dependencies from 293 to 73 K for S2 are presented in Figure 6a,b,c for the "high","transitional" and "low" temperature ranges. With decreasing temperature, the mobility goes through a minimum at 253−233 K (Figure 6b) and then increases, to the lowest temperature yet obtained of 73 K (Figure 6c). Results from 253 to 73 K were reversible but with a hysteresis of several hours.

The field and temperature dependencies of mobility were similarly investigated for S3 (T_s = 95 °C, rate = 200 Å/min), with the results appearing in Figures 7 and 8a,b and Table 1. The ln μ versus $E^{1/2}$ plots in Figure 7 at the high temperature range of 333−273 K show an inverse mobility dependence on field for most of the field range investigated. By contrast, such a predominantly inverse field dependence is only observed at certain low temperatures for S2 (Figure 6) and not at all for S1 (Figure 4). The temperature range conforming to the formalism was further restricted by 20 K in this sample, since for T_m = 333 K the mobility at high fields is field-independent. The calculations performed from Figure 7 are therefore on a minimal data base. Agreement with the dependencies predicted by the formalism remained excellent in this limited range.

In Figure 8a, *mobility in S3 reverses both its temperature and field dependencies at 253 K.* The inverse dependencies continue in Figure 8b in the lower range T_m = 253−213 K. Due to the resolution of the experimental apparatus (∼200 ns), no mobility values could be obtained at temperatures below 213 K or at higher fields than those depicted.

B. Electron Mobilities. Electron mobilities were measured over a similar range of fields and all temperatures for S1 and

TABLE 1: Comparison of Disorder Parameters from Hole Mobilities in the Present Sample Types S1−S3 and Relevant Previous Samples C1 and C2

sample type	σ (eV)	Σ	C	μ_o (cm^2/(V s))	μ_{00} (cm^2/(V s))
S3 (T_s = 95 °C, rate 200 Å/min)	0.0524	1.85	9.4×10^{-4}	5.0×10^{-3}	9.0×10^{-4}
S2 (25 °C, 200 Å/min)	0.0645	2.22	9.5×10^{-4}	9.1×10^{-3}	7.7×10^{-4}
S1 (95 °C, 1100 Å/min)	0.0726	2.18	9.5×10^{-4}	6.5×10^{-3}	6.0×10^{-4}
C2 (95 °C, 200 Å/min)	0.0778	1.87	1.0×10^{-3}	2.1×10^{-3}	3.6×10^{-4}
C1 (25 °C, 200 Å/min)	0.1013	2.76	8.5×10^{-4}	4.8×10^{-3}	1.1×10^{-4}

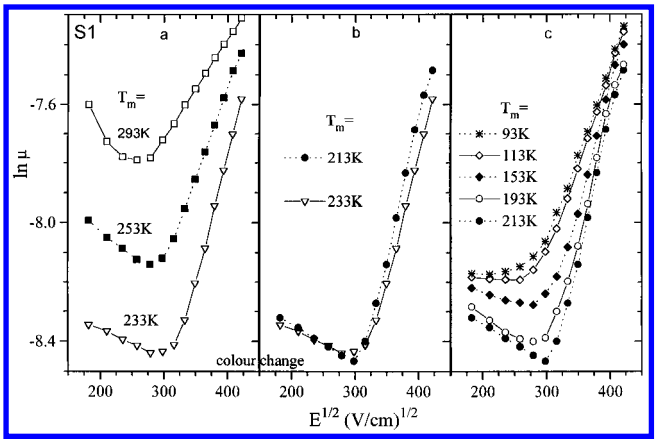

Figure 4. Reversal of hole mobility with decreasing temperature for S1 (T_s = 95 °C, rate = 1000 Å/min). (a) Activated mobility temperature dependence illustrated from T_m = 293 K to 233 K; (b) transition in mobility temperature dependence from T_m = 233 to 213 K; (c) increasing mobilities with decreasing temperature from T_m = 213 to 93 K.

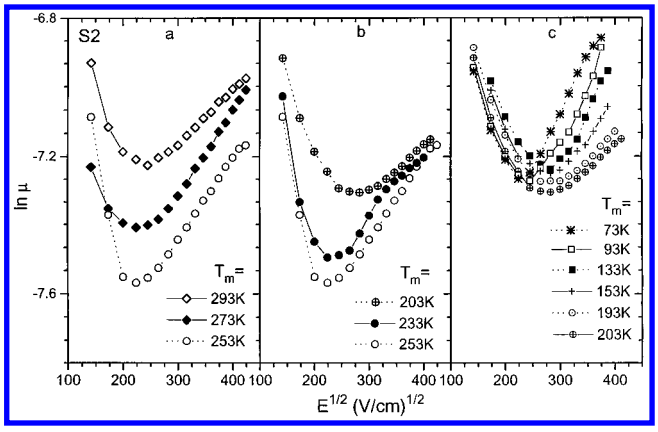

Figure 6. Reversal of hole mobility behavior with decreasing temperature for S2 (T_s = 25 °C, rate = 200 Å/min). (a) Activated mobility temperature dependence illustrated from T_m = 293 K to 253 K; (b) transition in mobility temperature dependence from T_m = 253 to 203 K; (c) increasing mobilities with decreasing temperature from T_m = 203 to 93 K.

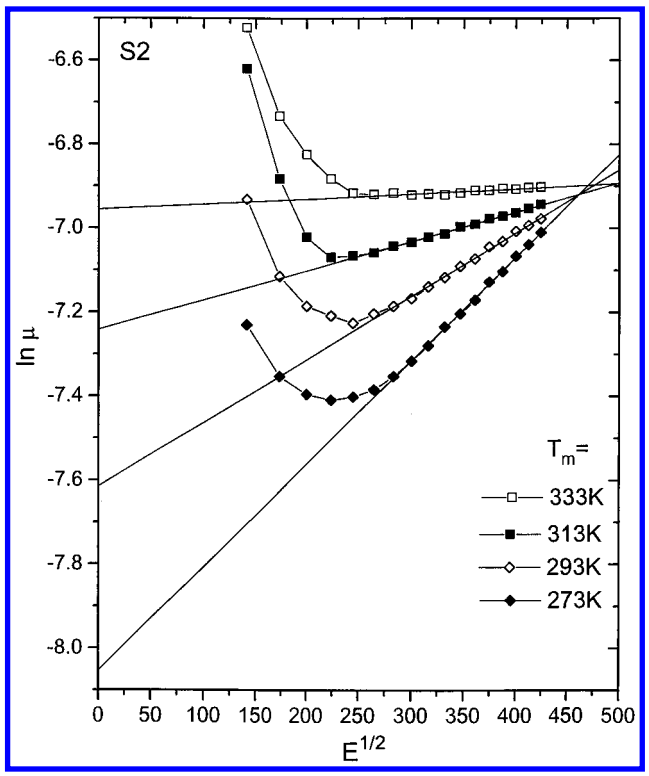

Figure 5. Field dependence of hole mobility at high temperatures T_m = 333−273 K for S2 (T_s = 25 °C, rate = 200 Å/min). The relation ln $\mu \propto E^{1/2}$ is followed for E above ~6.2 × 10^4 V/cm. An inverse field dependence applies for E below (5−6) × 10^4 V/cm.

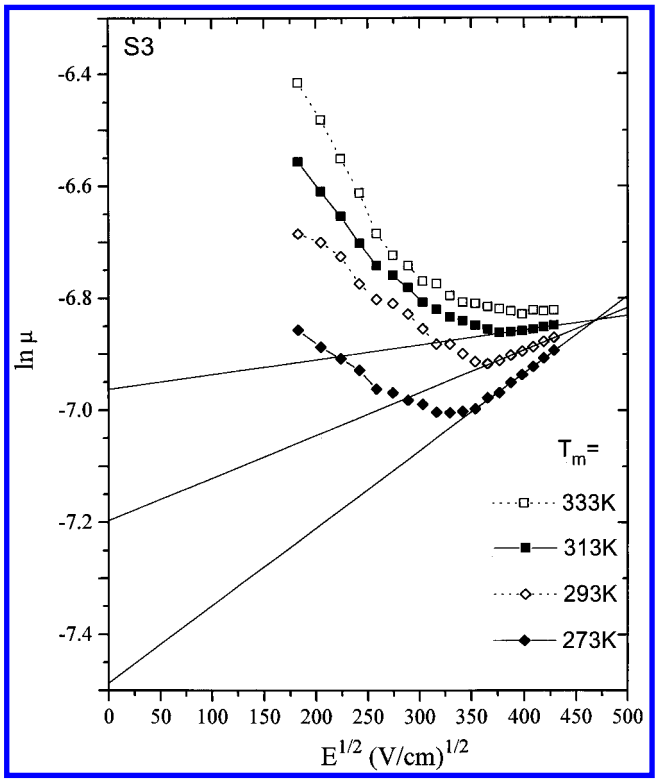

Figure 7. Field dependence of hole mobility at high temperatures T_m = 333−273 K for S3 (T_s = 95 °C, rate = 200 Å/min). The relation ln $\mu \propto E^{1/2}$ is followed for E above ~1.25 × 10^5 V/cm. An inverse field dependence is observed for E below ~1.2 × 10^5 V/cm.

S3. Figure 9 shows a typical electron transient at a field of 8 × 10^4 V/cm and a comparable hole transient at the corresponding field for the same sample (S1). Similarities and differences in hole and electron transients are (i) electron photocurrent and dispersivity closely approaches that of hole transients at fields above ~5 × 10^4 V/cm; (ii) the inverted electron transients only appear at fields greater than ~1.5 × 10^4 V/cm, and the photocurrent at such low fields is smaller than that of hole transients by over an order of magnitude; and (iii) samples had to be short-circuited between any two measurements, as there were changes in photocurrent and dispersivity.

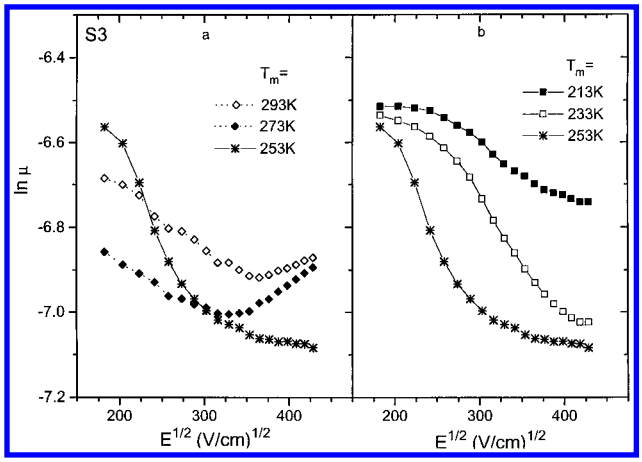

Figure 8. Reversal of hole mobility with decreasing temperature for S3 (T_s = 95 °C, rate = 200 Å/min). (a) Activated mobility temperature dependence applies only down to T_m = 273 K; transition observed in mobility temperature dependence and field dependence at T_m = 253 K. (b) Increasing mobilities with decreasing temperature from T_m = 253 to 213 K.

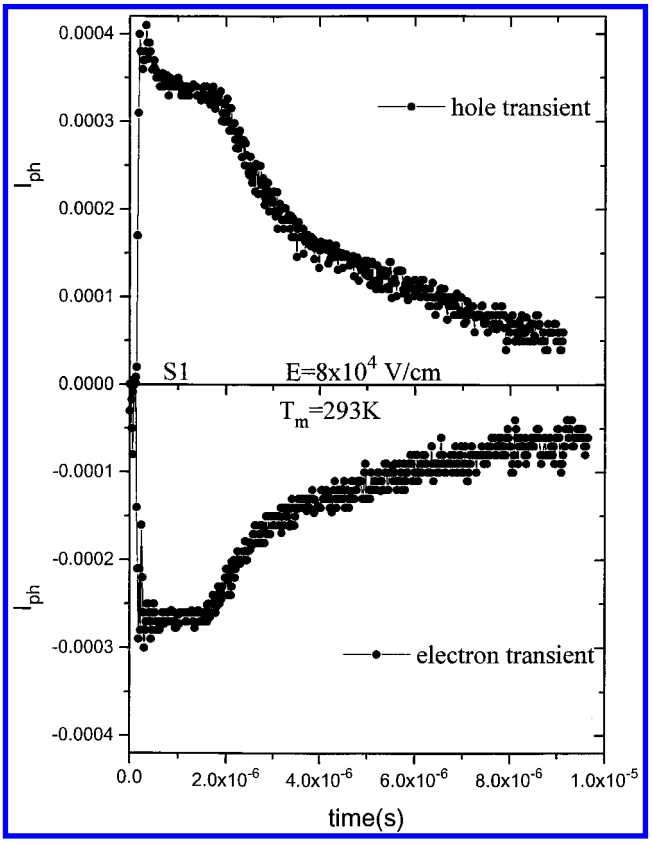

Figure 9. Comparison of electron and hole transients in S1 at the same experimental conditions, $E = 8 \times 10^4$ V/cm and T_m = 293 K.

Figure 10 shows the field dependence of electron mobility at T_m = 333−253 K for S1. The results follow the predictions of the disorder formalism. Parameters are compared in Table 2 to those obtained from hole mobilities in the same sample.

The field dependence of electron mobilities at T_m = 293−113 K for S1 are illustrated in Figure 11a,b,c. Figure 11a shows the mobility goes through a minimum at 233 K. In Figure 11b, from 233−193 K the electron *mobility reverses both its temperature and its field dependencies for most of the field range*. These dependencies continue in Figure 11c.

The field dependence of electron mobility for S3 appears in Figure 12a,b. *The field dependence of mobility was inverse or flat throughout the entire field range observed and for all*

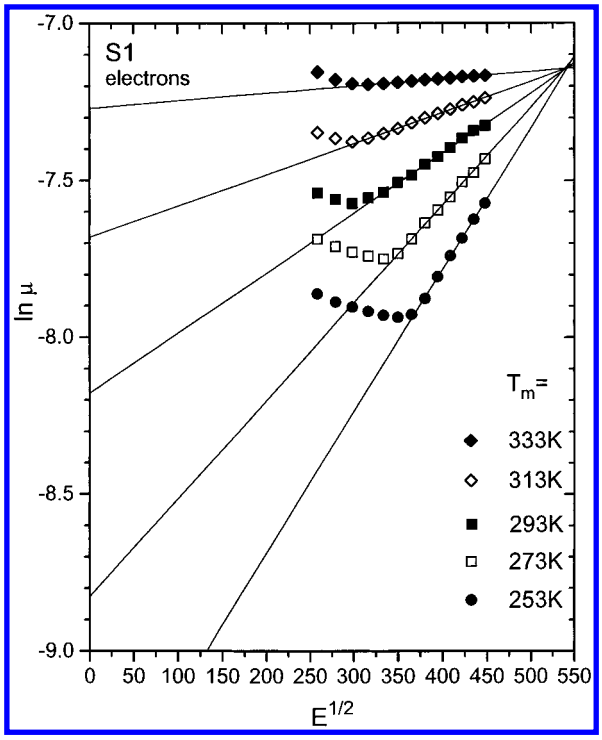

Figure 10. Field dependence of electron mobilities at high temperatures T_m = 333−253 K for S1 (T_s = 95 °C, rate = 1000 Å/min). The relation ln $\mu \propto E^{1/2}$ applies for E above ~1 × 10^5 V/cm. An inverse field dependence is observed for E below ~(0.9−1) × 10^5 V/cm.

TABLE 2: Comparison of Disorder Parameters Obtained in the Same Sample, S1, According to Hole and Electron Mobility Results

carriers	σ (eV)	S	C	μ_o (cm^2/(V s))	μ_{00}(cm^2/(V s))
holes	0.0726	2.18	9.5×10^{-4}	6.5×10^{-3}	6.0×10^{-4}
electrons	0.0760	2.65	8.3×10^{-4}	1.6×10^{-2}	5.5×10^{-4}

temperatures. Accordingly, disorder parameters could not be calculated. A reversal of the temperature dependence of mobility at the higher fields is noted in Figure 12b from T_m = 273−213 K.

Finally, both S1 and S3 were tested in air for electron transients. A response was only observed above relatively large fields of ~1.2 × 10^5 V/cm and was very dispersive. For freshly prepared samples at T_s = 25 °C, rate = 2000 Å/min, in air, there were no electron transients. In vacuum, a weak response appeared at large fields above ~2 × 10^5 V/cm. The observation of an electron photocurrent shows therefore a dependence on sample type as well as on environmental conditions.

Discussion

A. Hole Transport. The hole mobility dependencies at the higher end of the temperature range investigated for S1, S2, and S3 (Figures 3, 5, and 7) were in good agreement with predictions of the disorder formalism. Firstly the relation ln$\mu \propto SE^{1/2}$ is observed at high fields, and μ passes through a minimum at lower fields. Secondly, the high-field slopes increase with decreasing temperatures and are in excellent agreement with the $1/T^2$ relation proposed by the formalism. Thirdly, the temperature dependence of ln μ is also in excellent agreement with $1/T^2$ for all samples (standard deviations of <0.001). This also means that any Arrhenius plot of ln μ versus $1/T$ shows some curvature. However, the latter is by no means a convincing distinction between the two temperature dependencies as the temperature range is too short.

The observed dependencies support the expectation that the formalism provides a meaningful framework for the discussion

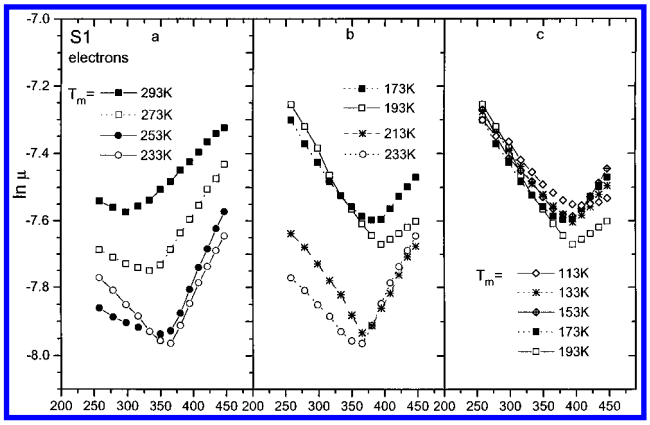

Figure 11. Reversal of electron mobility with decreasing temperature for S1 (T_s = 95 °C, rate = 1000 Å/min). (a) Activated mobility temperature dependence illustrated from T_m = 293 K to 253/233 K; (b) transition in mobility temperature dependence occurs from T_m = 233/213 K to 193/173 K; (c) increasing or stable mobilities with decreasing temperature from T_m = 193 to 113 K.

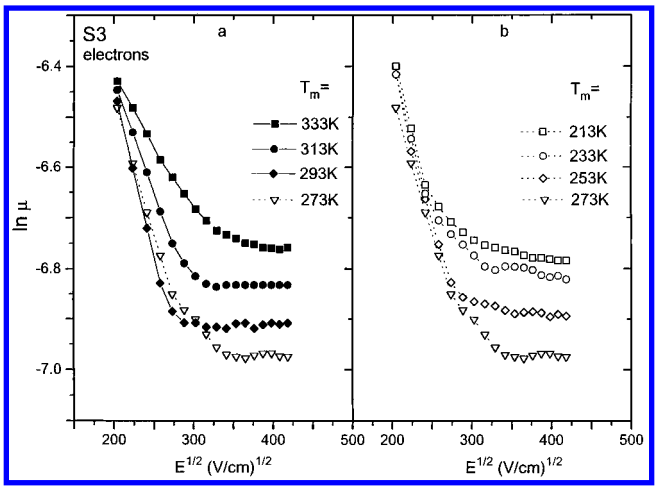

Figure 12. Inverse field dependence of electron mobilities for S3 (T_s = 95 °C, rate = 200 Å/min) at both (a) high temperatures T_m = 333−273 K and (b) low temperatures T_m = 273−213 K.

of hole transport at high temperatures. A discussion of all parameters and self-consistency relations within the formalism and of trends for both hole and electron mobilities follows.

The parameters of the formalism. Table 1 shows a significant *decrease in σ on going from S1 to S3* (∼28%). At the same time, Σ does not show any consistent trend from S1 to S3, fluctuating about a mean value of ∼2.0. The smaller value of σ implies less energetic disorder $\hat{\sigma}$ at any given temperature of comparison (recall eq 3). The mobility therefore should increase from S1 to S3 at any given T_m. Similarly, the slopes of $\ln \mu \propto SE^{1/2}$ should decrease from S1 to S3 at any given T_m. These trends across sample types are confirmed, appearing most clearly in Figure 2, where the constant T_m means that $\hat{\sigma}$ decreases from the lower to upper curves in this figure.

The higher values of μ are not accounted for solely by the resultingly smaller $\hat{\sigma}$ at a given temperature, since then mobilities for different samples should be the same if compared at the same values of $\hat{\sigma}$ and Σ. That this is not the case can be seen from S1 (Figure 3) and S2 (Figure 5), which have nearly identical Σ values (Table 1). At, for example, T_m = 333 K and T_m = 293 K, respectively, $\hat{\sigma}$ are also nearly identical. Yet, mobilities for S2 at 293 K are still larger than for S1 at 333 K, despite the identical set of disorder parameters ($\hat{\sigma}$, Σ).

This indicates that the expected change in film morphology, which in the present samples narrows the width of the distribution of states, has a further, underlying, effect on the charge transport. This underlying effect appears when calculating the mobility at zero field, infinite temperature, and no disorder, μ_{00}, which is given by the formalism as

$$\mu_o = \mu_{00} \exp(\Sigma^2/2) \qquad (4)$$

The μ_{00} in eq 4 contains a dependence on wave function overlap.[36] A change then in μ_{00} should reflect a change in the orbital overlap of the phthalocyanine macrocycles, the accepted sites of hole transport in these materials.[37,38] The increasing trend in μ_{00} from S1 → S3 is very evident in Table 1. Furthermore, comparison with results for variously less organized films previously studied (for example C1 and C2) shows this trend of increasing μ_{00} with increasing measured mobilities to be consistent for all ClAlPc films studied to date.[20] Therefore, the improvement in mobilities depicted in Figure 2 results from an increase in μ_{00} and a decrease in σ.

The trend in μ_{00} as well as the decrease in σ have been correlated to aggregation and short-range order (microcrystallites), which are created in ClAlPc films for substrate temperatures of T_s = 95 °C,[20] as detected by transmission electron microscopy (TEM).[22] When aggregates form, there is a better overlap of the wave functions of neighboring molecules, increasing μ_{00}, and the interactions of a carrier with its surroundings are "averaged" over a few molecules. This decreases the variety of surroundings about each site or width of the distribution of states.[39,40]

Reversal of Mobility at Low Temperatures. The present results verify the occurrence of a mobility that increases with decreasing temperatures in a low-temperature range (Figures 4, 6, 8). In addition, when comparing S1, S2, and S3 in Figures 4b, 6b, and 8a, the point at which μ starts to rise with decreasing temperature (the reversal temperature) shifts to higher T_m: 213 → 233 → 253 K, respectively. This trend is consistent with previous results where less ordered films showed a reversal temperature of 193/200 K.[21] It was suggested that the mobility increase at low temperatures is caused by a shift of Pc macrocycles toward a greater cofacial overlap on cooling, which would increase mobility. This was supported by absorbance measurements, where at the same low temperatures, a blue broadening was observed that is widely identified in the literature with just such an interplanar shifting. The trend now of increasing reversal T_m from 213 to 253 K for S1−S3 may be understood in light of the μ_{00} results: if macrocycles are already in closer proximity as a result of molecular aggregation, a greater cofacial overlap on cooling could be achieved at higher T_m.

Finally, improved molecular overlap, whether at low temperatures or as a result of changing deposition conditions, correlates to the increasingly inverse field dependencies which are observed from S2 to S3 over widening T_m ranges (Figures 6, 7, 8).

B. Electron Transport. The inverted transients obtained when the illuminated electrode is negative are very similar to the hole transients. The assignment of inverted transients to electron transport is therefore straightforward, and interpretation of the drift mobilities calculated from them should be comparable to the usual hole transients.

The following observations regarding both the electron photocurrent and mobility are unusual. The first observation on obtaining an electron response was the similarity of electron transients at fields ≥5 × 10^4 V/cm to those of holes at similar fields, as illustrated in Figure 9. This applies both to photocurrent (it approaches 2/3 that of holes at the highest fields) and to the moderate dispersivity of transients. Molecular oxygen is known to trap electrons in MPc,[3b] as in most organic

materials,[41,42] and electron transients are usually observed only in very pure single crystals where extreme care has been taken to avoid exposure to air.[41] While the ClAlPc presently used is indeed well purified, the samples are certainly not single crystals and moreover were exposed to air in between the sample preparation stages. The measurement chamber primary vacuum of $10^{-3}/10^{-2}$ Torr did make a difference to size and dispersivity of transients in S1−S3, leading to the conclusion that it is effective in causing some degassing of adsorbed oxygen. The degassing however was not effective in enabling mobility measurements for films sublimed with greater amounts of disorder (such as C1 in Table 1). These materials could display a larger variety of oxygen-trapping sites compared to more organized materials.

The second observation is that electron mobilities are very similar to hole mobilities in any given sample (compare for example S1 electron mobilities in Figure 10 to S1 hole mobilities in Figure 3). Literature reports on electron transport in organic materials usually show orders of magnitude lower mobilities for electron versus hole transport. Molecular glasses of NTDI [*N*,*N*′-bis(1,2-dimethylpropyl)-1,4,5,8-naphthalenetetracarboxylic diimide] have the highest electron mobility ($\mu \approx 4 \times 10^{-5}$ cm^2/(V s) among currently known electron transport amorphous molecular solids.[18,43] However, low electron mobilities more commonly obtained are attributable to a structural difference between two types of materials studied: Electron transport is seen in acceptor molecules which usually have functionalities with large group dipole moments compared to hole-transporting donor molecules.[44] There is thus a large dipolar contribution to the total σ in films of acceptor molecules according to the relation[45] $\sigma^2_{\text{Total}} = \sigma^2_{\text{vanderWaals}} + \sigma^2_{\text{Dipolar}}$. In the present case, the same material is studied so that no such structural differences come into play to decrease electron mobility. This however does not mean that the transport environment is identical in ClAlPc for holes and electrons, as will be seen below.

Parameters of the Formalism. In Table 2, the σ obtained from hole and electron data in the same sample, S1, is very similar, but Σ shows a marked increase for electrons (18% larger). This may reflect an expected difference in charge transport sites for holes and electrons in Pcs similar to ClAlPc. In $[Si(Pc)O]_n$[46] and $Si(Pc)(OH)_2$,[47] molecular orbital calculations show that the highest occupied molecular orbital is comprised entirely of out-of-plane p_z atomic functions of the Pc ring (the π-state) and so has no amplitude on the central metal or oxygen. Conversely, the lowest unoccupied molecular orbital, comprised of the excited π*-state, has a considerable amount of silicon−oxygen π-bonding character. These orbital configurations should apply to any MPc, including ClAlPc, where the HOMO is due to the π-state and the LUMO to the π*-state.[3,46,47] Therefore, holes are restricted to the Pc ring, while electron transport should also involve orbitals at the Al−Cl bond. Since Σ is a function of charge transfer integrals and intermolecular configurations, this parameter may be the more likely one to reflect a greater variety of orbitals involved in electron transport.

Reversal of Mobility at Low Temperatures. Figure 11 shows an increase in electron mobility at low temperatures for S1, at approximately the same reversal T_m as for holes. This agrees with the link of reversal temperature to orbital overlap, as the μ_{00} for electrons is very similar to that of holes (5.5×10^{-4} and 6×10^{-4} cm^2/(V s, respectively, in S1). For S3 (Figure 12) the mobility reversal again appears, but only at high fields. The field dependencies of mobility are predominantly inverse both above and below the reversal temperature for S3.

According to the preceding discussion, the possibility emerges of a transition in charge transport mechanism. The energetic disorder becomes especially small by S3, wave function overlap increases, and mobility field dependencies become more negative, which may reflect a transition away from hopping that is controlled by energetic disorder.

Conclusion

The study of charge transport in thin films of ClAlPc vacuum sublimed under different combinations of substrate temperature and sublimation rate reveals an improvement in hole mobilities up to 10^{-3} cm^2/(V s) for the combination (S3) of lowest rate = 200 Å/min and highest T_s = 95 °C. Field and temperature dependencies of hole mobility were very well described by the formalism of disorder of Bässler and co-workers. The disorder parameters can be said to give a relative picture of the evolution of the transport environment with film deposition conditions. Accordingly, the transport environment is becoming less energetically disordered from S1 to S3, with σ, the width of the DOS, varying from 0.0726 to 0.0520, respectively. The average molecular orbital overlap is also increasing, according to μ_{00}, which increases from 6 to 9×10^{-4} cm^2/(V s) from S1 to S3. The correlation of parameters and increased mobilities is consistent with results of previous studies and therefore suggests agglomeration of molecules and even increased microcrystallite formation from S1 to S3. A reversal in temperature dependence of mobility is observed in all samples at a low temperature. This reversal temperature rises with increased molecular orbital overlap from S1 to S3, reaching 253 K. Cooling the films is thought to further increase the coplanar overlap of Pc macrocycles. Greater orbital overlap is correlated then to a trend of increasingly inverse field dependencies.

Unusually high electron mobilities are measured in amorphous/polycrystalline thin films of ClAlPc without the need of any specific film treatments. Electron mobilities have magnitudes comparable to the hole mobilities and increase from S1 to S3. The formalism reveals similar σ and μ_{00} for S1, but increased positional disorder Σ. It is suggested that this may reflect a difference in transport sites for electron and hole transport as deduced from molecular orbital calculations in the literature. Trials in air and on less organized samples previously studied indicate that, apart from the environment, the molecular packing plays an important role in electron transport for ClAlPc thin films. Other trivalent metal phthalocyanines or even oxotitanyl phthalocyanine, materials of packing similar to ClAlPc,[48] are expected to show comparable electron transport behavior.

Acknowledgment. The authors would like to thank Paul Borsenberger for continued helpful discussions. The synthesis of chloroaluminum phthalocyanine by Roland Côté is gratefully acknowledged. This study was supported by the National Science and Engineering Research Council of Canada.

References and Notes

(1) Gregory, P. *High-Technology Applications of Organic Colorants*; Plenum Press: New York, 1991.

(2) Leznoff, C. C., Lever, A. B. P., Eds. *Phthalocyanines, Properties and Applications;* VCH: Weinheim, Vol. 1, 1989; Vol. 2, 1993; Vol. 3, 1994; Vol. 4, 1996.

(3) Simon, J.; André, J. J. *Molecular Semiconductors*; Springer-Verlag: Berlin, 1985; (a) p 107; (b) p 112.

(4) Popovic, Z. D. *J. Chem. Phys.* **1982**, *76*, 2714.

(5) Popovic, Z. D. *J. Chem. Phys.* **1983**, *78*, 1552.

(6) Popovic, Z. D. *Chem. Phys.* **1984**, *86*, 311.

(7) Popovic, Z. D.; Hor, A. M. *Proc. SPIE (Fluorescence Detection II*) **1988**, *910*, 168.

(8) Popovic, Z. D.; Mesbah, S. *Chem. Phys. Lett.* **1993**, *215*, 636.

(9) Cox, G. A.; Knight, P. C. *J. Phys. C: Solid State Phys.* **1974**, *7*, 146.

(10) Petit, P.; Turek, Ph.; André, J. J.; Even, R.; Simon, J. *Synth. Met*. **1989**, *29*, F59.
(11) Waclawek, W.; Zabrowska-Waclawek, M. *Thin Solid Films* **1987**, *146*, 1.
(12) Shihub, S. I.; Gould, R. D. *Thin Solid Films* **1995**, *254*, 187.
(13) Meyer, J. P.; Schlettwein, D.; Wöhrle, D.; Jaeger, N. I. *Thin Solid Films* **1995**, *258*, 317.
(14) Ziolkowska-Pawlak, B.; Mycielski, W. J. *Non-Cryst. Solids* **1987**, *90*, 645.
(15) Schouten, P. G.; Warman, J. M.; deHaas, M. P.; van Nostrum, C. F.; Gelinck, G. H.; Nolte, J. M. R.; Copyn, M. J.; Zwikker, J. W.; Engel, M. K.; Hanack, M.; Chang, Y. H.; Ford, W. T. *J. Am. Chem. Soc*. **1994**, *116*, 6880.
(16) Groothues, H.; Kremer, F.; Schouten, P. G.; Warman, J. M. *Adv. Mater*. **1995**, *7*, 283.
(17) Dumm, M.; Lunkenheimer, P.; Loidl, A.; Assman, B.; Homborg, H.; Fulde, P. *J. Chem. Phys*. **1996**, *104*, 5048.
(18) Borsenberger, P. M.; Weiss, D. S. *Organic Photoreceptors for Imaging Systems*; Marcel Dekker: New York, 1993.
(19) Devaux, P.; Quedec, P. *Phys. Lett*. **1969**, *28A*, 537.
(20) Ioannidis, A.; Dodelet, J. P. *J. Phys. Chem*. **1997**, *101*, 891.
(21) Ioannidis, A.; Dodelet, J. P. *J. Phys. Chem*. **1997**, *101*, 901.
(22) Santerre, F.; Côté, R.; Saint-Jacques, R. G.; Dodelet, J. P. *J. Phys. Chem*. **1996**, *100*, 7632.
(23) Gastonguay, L.; Veilleux, G.; Côté, R.; Saint-Jacques, R. G.; Dodelet, J. P. *J. Electrochem. Soc*. **1992**, *139*, 337.
(24) Movaghar, B.; Grünewald, M.; Ries, B.; Bässler, H.; Wurtz, D. *Phys. Rev. B* **1986**, *33*, 5545.
(25) Richert, R.; Bässler, H.; Ries, B.; Movaghar, B.; Grünewald, B. *Phil. Mag. Lett*. **1989**, *59*, 95.
(26) Bässler, H. *Phys. Status Solidi* **1993**, *B175*, 16.
(27) Frenkel, J. *Phys. Rev*. **1938**, *54*, 647,
(28) Borsenberger, P. M.; Pautmeier, L. T.; Bässler, H. *J. Chem. Phys*. **1991**, *94*, 5447.
(29) Pautmeier, L.; Richert, R.; Bässler, H. *Synth. Met.* **1990**, *37*, 271.
(30) Borsenberger, P. M.; Pautmeier, L. T.; Bässler, H. *Phys. Rev. B* **1992**, *46*, 12145.
(31) Owens, J. E.; Kenney, M. E. *Inorg. Chem*. **1962**, *1*, 331.
(32) Dolezalek, F. K. In *Photoconductivity and Related Phenomena*; Mort, J., Pai, D. M., Eds., Elsevier Scientific: Amsterdam, 1976; p 27.
(33) Melnyk, A.; Pai, D. M. In *Physical Methods of Chemistry*; Baetzold, R., Hamilton, J., Rossiter, B., Eds.; John Wiley: New York, 1993; Vol. 8, Chapter 5.
(34) Schein, L. B. *Phil. Mag.* **1992**, *B65*, 795.
(35) Borsenberger, P. M.; Magin, E. H.; van der Auweraer, M.; deSchryver, F. C. *Phys. Status Solidi* **1993**, *140a*, 9.
(36) Pautmeier, L.; Reis, B.; Bässler, H. *Chem. Phys. Lett*. **1988**, *143*, 459.
(37) Marks, T. J. *Science* **1985**, *227*, 881.
(38) Orti, E.; Brédas, J. L. *Synth. Met.* **1989**, *33*, 27.
(39) Young, R. H.; Fitzgerald, J. J. *J. Phys.Chem*. **1995**, *99*, 4230.
(40) Gartstein, Yu. N.; Conwell, E. M. *Chem. Phys. Lett*. **1995**, *245*, 351.
(41) Pope, M.; Swenberg, C. E. *Electronic Processes in Organic Crystals*; Oxford University Press: Oxford, 1982.
(42) Silinsh, E. A.; Cápek, V. *Organic Molecular Crystals*; AIP: Williston, VT, 1994.
(43) Borsenberger, P. M.; Gruenbaum, W. T.; Magin, E. H. *Phys. Status Solidi B* **1995**, *190*, 555.
(44) O'Regan, M. B.; Borsenberger, P. M.; Gruenbaum, W. T. *Phys. Status Solidi* **1995**, *148a*, 259.
(45) Borsenberger, P. M.; Gruenbaum, W. T.; Magin, E. H.; Sorriero, L. J. *Chem. Phys*. **1995**, *195*, 435 (and references therein).
(46) Ciliberto, E.; Doris, K. A.; Pietro, W. J.; Reisner, G. M.; Ellis, D. E.; Fragal, I.; Herbstein, F. H.; Ratner, M. A.; Marks, T. J. *J. Am. Chem. Soc*. **1984**, *106*, 7748.
(47) Hale, P. D.; Pietro, W. J.; Ratner, M. A.; Ellis, D. E.; Marks, T. J. *J. Am. Chem. Soc.* **1987**, *109*, 5943.
(48) Ghosez, Ph.; Côté, R.; Gastonguay, L.; Veilleux, G.; Denes, G.; Dodelet, J. P. *Chem. Mater*. **1993**, *5*, 1581.